# Study of Fluid Flow through Scaled-up Ink Jet Nozzles

Abstract: A 100-fold scaled-up model of ink jet nozzle flow is described. A theoretical justification for scaling the relevant parameters, starting from the equations of motion, is presented. The scaling procedure and the effects of unscaled parameters are discussed as well as the scaled-up "ink." Following a description of the experimental apparatus, the results of a series of experiments are then presented. These consist of directionality, directional stability and flow efficiency measurements in four nozzle configurations: conical, cylindrical, square, and "hybrid" nozzles.

#### Introduction

Ink-jet printing is a newcomer to the family of printers. Extremely small nozzles (typically 25-50  $\mu$ m diameter) emit fine jets of ink which break up into small droplets, 50-100  $\mu$ m in diameter. These droplets are individually charge-labeled at their breakoff time and then deflected to the appropriate position on paper. The small size of the nozzles makes them difficult to manufacture reproducibly, and also makes the identification of sources of variable performance difficult to diagnose.

The possibility of studying fluid flow through properly scaled-up nozzles suggests itself and is especially attractive because it permits investigation under controlled experimental conditions. It is, however, impractical (and in most cases impossible) to scale up all the parameters characterizing a physical system. Instead a simple model, describing the phenomenon with a minimum number of parameters, is normally used. Furthermore, only the relevant parameters need be scaled; the effects of unscaled parameters need only be sufficiently understood so that they can be either corrected for or ignored. The Navier-Stokes equations, based on such a model of fluid flow, are presented below. The relevant parameters are found to be those describing viscosity effects, surfacetension effects, and gravity effects. It is then shown that viscosity and surface tension effects can be properly scaled up, whereas gravity cannot. The scale-up factor itself is then discussed. The tendency is to choose a scale factor as large as possible to permit easy control of nozzle characteristics, thus making systematic measurements possible. However, a scale factor that is too large results in an unusually sensitive jet coupled with large gravity effects. A scale-up factor of 100 seems to be an acceptable compromise.

Because gravity continuously modifies the jet's exponential instability factor, it was decided to concentrate

on flow efficiency and jet directionality effects with different nozzle configurations. A smaller scale model of an ink jet, in which gravity effects are of lesser importance, is described in [1]. There, jet stability problems and drop formation are analyzed.

Data presented here were obtained from four different nozzle configurations. These include conical, cylindrical, square and a "hybrid" configuration in which a square entrance leads the flow into a circular cylindrical orifice. Discussion is limited to the cylindrical nozzles, the configuration most easily treated analytically. A direct comparison among the four nozzle configurations was purposely avoided because it can be misleading to compare "ideal" nozzles that may have different manufacturability limits.

## Modeling and analysis

It is assumed that the fluid being investigated obeys the Navier-Stokes equations of motion [2]. These equations, which apply to all gases and most "simple" liquids, are based on the following properties: 1) The fluid is isotropic—i.e. has no preferred directions, 2) stress is a linear function of the deformation rates, and 3) stress must reduce the hydrodynamic pressure in the absence of deformation.

The dye-based inks used in some ink-jet printing are dilute polymer solutions in water. Their viscosity is a weak function of shear rate [3] and consequently can be approximated by a Newtonian (constant viscosity) fluid. Like most liquids these inks are also incompressible.

# • The Navier-Stokes equations

With the assumptions given above, the equations of motion can be written as:

56

$$\rho \frac{dv_i}{dt} = \rho \left( \frac{\partial v_i}{\partial t} + v_k \frac{\partial v_i}{\partial x_k} \right)$$

$$= \rho g_i - \frac{\partial p}{\partial x_i} + \mu \frac{\partial^2 v_i}{\partial x_k \partial x_k} \cdots, \quad i, k = 1, 2, 3, \tag{1}$$

where the summation convention (over repeated indices) is used, and  $\rho$  is density,  $\mu$  is dynamic viscosity, p is pressure,  $v_i$  is the velocity component along the  $x_i$  axis, and  $g_i$  is the acceleration component (due to gravity) in the  $x_i$  direction. Note that Eq. (1) is simply Newton's second law ( $\mathbf{F} = m\mathbf{a}$ ), applied to a unit volume of the fluid. Here gravity is the only "external" force present.

The velocity v is constrained by the continuity equation (conservation of mass) which, for an incompressible flow, takes the form

$$\partial v_k / \partial x_k = 0. (2)$$

- · Boundary conditions
- 1. Inside the nozzle (nonslip):

$$v_i(\mathbf{r})|_{\mathbf{r}=\mathbf{R}_v}=0,\tag{3}$$

in which  $\mathbf{R}_{N}$  is the radius-vector to the nozzle wall.

2. Outside the nozzle:

$$-\rho \delta_{ik} + \mu \left[ \frac{\partial u_i}{\partial x_k} + \frac{\partial u_k}{\partial x_i} \right]_{P=R_j} = \tau_{ik} = \delta_{ik} \sigma \left( \frac{1}{R_1} + \frac{1}{R_2} \right) \hat{n}_i \cdot \cdot \cdot, \tag{4}$$

in which

$$\delta_{ik} = \begin{cases} 1 & i = k \\ 0 & i \neq k \end{cases};$$

 $\sigma$  is surface tension;  $R_1$ ,  $R_2$  are the principal radii of curvature at  $\mathbf{r} = \mathbf{R}_j$ , the jet's surface vector;  $n_i$  is the *i*th component of  $\hat{n}$ , the unit normal to the jet's surface at  $\mathbf{r} = \mathbf{R}_j$ , and  $\tau_{ik}$  are components of the stress tensor.

For a cylindrically symmetric nozzle of diameter  $d_{\rm N}$ , the boundary conditions (in cylindrical coordinates) simplify to

$$\left.v\right|_{r=d_N/2}=0$$

inside the nozzle, and

$$-p+2\mu\frac{\partial v_r}{\partial r}\Big|_{r=d,l^2}=\frac{2\sigma}{d};$$

$$\mu \left( \frac{\partial v_r}{\partial z} + \frac{\partial v_z}{\partial r} \right) \Big|_{r=d;/2} = 0$$

outside the nozzle.

## Dimensional analysis

The aforementioned equations can be brought into a dimensionless form as follows. Let

$$t^* = t/t_0$$
,  $v_i^* = v_i/v$  and  $x_i^* = x_i/d$ .

Choose  $p^* = p/\rho v^2$ ,  $R = \rho v d/\mu$ ,  $W = \rho v^2 d/\sigma$ ,

$$F = v^2 / gd$$
, and  $t_0 = (\rho d^3 / \sigma)^{\frac{1}{2}}$ .

The parameters d and v are the characteristic linear dimension and velocity, respectively, of the problem being studied. A specific characteristic time  $t_0$  was chosen, above, in anticipation of laminar jet-stability behavior. The other parameters are:

Reynolds number: 
$$R = \rho v d / \mu$$
 (viscosity effects), (5)

Weber number: 
$$W = \rho v^2 d / \sigma$$
 (surface tension

Froude number: 
$$F = v^2/gd$$
 (gravity effects). (7)

# • Equations of motion (dimensionless)

The Navier-Stokes equations, Eqs. (1) and (2), can now be rewritten as:

$$\frac{1}{W^{\frac{1}{2}}}\frac{\partial v_i}{\partial t^*} + v_k^* \frac{\partial v_i^*}{\partial x_k^*} = \frac{1}{F} \alpha_i - \frac{\partial p^*}{\partial x_k} + \frac{1}{R} \frac{\partial^2 v_i}{\partial x_k^* \partial x_k^*}; \tag{1*}$$

$$\frac{\partial v_k^*}{\partial x_k^*} = 0, \tag{2*}$$

where the  $\alpha_i$  is the direction cosine between the gravity and  $x_i$  directions. (The appearance of the Weber number in Eq.  $(1^*)$  is due to the choice of the characteristic time  $t_0$  and has no other significance here.)

#### Boundary conditions (dimensionless)

In terms of the dimensionless parameters the boundary conditions are given as

$$\begin{aligned} v_i^*|_{r^* = R_N^*} &= 0 \text{ (inside nozzle)}; \\ -p^* \delta_{ik} &+ \frac{1}{R} \left( \frac{\partial v_i^*}{\partial x_k^*} + \frac{\partial v_k^*}{\partial x_i^*} \right)_{r^* = R^*} \end{aligned}$$
(3\*)

$$= \tau_{ik}^* = \delta_{ik} \frac{1}{W} \left( \frac{1}{R_1^*} + \frac{1}{R_2^*} \right) \hat{n}_i \text{ (outside nozzle)}.$$

For a cylindrically symmetric nozzle, the dimensionless boundary conditions (in cylindrical coordinates) are:

 $v|_{r^*=k}=0$  (inside nozzle), and

$$-p+2\mu\frac{\partial v_i^*}{\partial r^*}\Big|_{r^*=\frac{1}{2}}=\frac{2}{W};$$

$$\mu \left( \frac{\partial v_r^*}{\partial z^*} + \frac{\partial v_z^*}{\partial r^*} \right) \Big|_{r^* = \frac{1}{2}} = 0, \text{ (outside nozzle)}$$

where it was assumed (for simplicity) that:  $d_N = d_1 = d$ .

(4\*)

## • Analysis

The dimensionless equations of motion, including their boundary conditions, Eqs. (1\*-4\*), reveal that fluid motion is completely determined by three parameters; the Reynolds number, Eq. (5), the Weber number, Eq. (6), and the Froude number, Eq. (7). Heat conduction effects can be neglected in ink-jet printing applications. (Nonisothermal fluid flow was investigated by Christiansen and Kelsey [4] with similar conclusions.) Therefore, to achieve true scaled-up conditions (within the assumptions made above) it is sufficient to keep these three dimensionless parameters (R, W and F) identical to the values obtained from the real ink-jet system. This is not an easy task because the choice of proper liquids is limited. Specifically, it is easy to satisfy the viscosity conditions because liquids of widely varying viscosities are readily available. However, the variation of surface tension among liquids is relatively very small. Water, for example  $[\sigma = 72 \text{ dynes/cm } (0.072 \text{ N/m})]$ , has one of the highest values, whereas most readily available liquids display surface tensions in the range of 30-70 dynes/cm (0.03-0.07 N/m). Another problem in scaling up surface tension effects arises from the dynamic nature of the ink jet. The dynamic surface tension of ink may be higher than that measured statically. This difference could result from the fact that it takes time for the water-soluble ink components to reach the newly formed jet surface. This hypothesis has not been proved as yet and the static surface tension has been chosen to be used in the scaling processes [3].

In general, the Reynolds, Weber and Froude relationships, Eqs. (5), (6) and (7), are three scaling requirements. Once the geometric scale-factor is determined, the only scaling controls left are the velocity and the choice of fluids. Hence, the difficulty appears in finding a scaling liquid satisfying all R, W and F relationships.

# The scaling-up process

The fluid model described above applies to incompressible, Newtonian and isothermal fluid flow. Watersoluble dye-based inks are a reasonably good approximation to such a case. Fluid flow in this case is controlled by the three (dimensionless) parameters R, W and F as mentioned above.

# • Scaling procedure

In scaling-up problems, the linear dimensions are to be scaled up by a factor x. Let primed quantities refer to the scaled-up system. Then:

1. If R, W and F are all to be fixed,

$$d' = xd$$

$$v' = x^{\frac{1}{2}}v$$
 from Eq. (7) (Froude),

$$(\mu/\rho)' = x^{\frac{3}{2}}(\mu/\rho)$$
 from Eq. (5) (Reynolds), and

$$(\sigma/\rho)' = x^2(\sigma/\rho)$$
 from Eq. (6) (Weber).

2. If only R and W are to be fixed and  $(\sigma/\rho)$  is a constant,

$$d' = xd$$

$$v' = x^{-\frac{1}{2}}v$$
 from Eq. (6) Weber,

$$(\mu/\rho)' = x^{\frac{1}{2}}(\mu/\rho)$$
 from Eq. (5) Reynolds, and

$$(\sigma/\rho)' = (\sigma/\rho)$$
, but now,

$$F' = x^{-2}F$$
 from Eq. (7).

In choosing the optimal scaling factor x, the desire to make x as large as possible is offset by the desire to minimize sensitivity to the (ever present) low-frequency vibrations that affect jet stability. A scaled-up factor of x=100 has been chosen as the best compromise. For case 1) above, with x=100, d'=100d; v'=10v,  $(\mu/\rho)'=1000(\mu/\rho)$  and  $(\sigma/\rho)=10000$   $(\sigma/\rho)$ . A scaled-up fluid with the correct viscosity relationship may be found, but the surface tension requirement renders this case impractical. Consequently, fixing R, W and F cannot be achieved for a scaling factor of x=100. For case 2) above, with x=100, d'=100d; v'=1/10 v,  $(\mu/\rho)'=10(\mu/\rho)$  and  $(\sigma/\rho)'=(\sigma/\rho)$ .

In this case the viscosity and surface-tension requirements can be easily met. However, it should be noted that now  $F' = 10^{-4} F$ . The scaling effects on other parameters, for a scaling-up factor of 100, can now be derived based on case 2).

Time For d' = 100d; v' = (1/10) v and the period T' = 1000 T; therefore the frequency is scaled down by a factor of 1000; i.e. a scaled-up system frequency of 100 Hz corresponds to a typical ink jet excitation frequency of 100 kHz.

*Pressure* Since  $p/\rho v^2$  is dimensionless, p scales as  $v^2$  so that p' = (1/100) p, i.e., low pressures are required for the 100-fold scaled-up system (0.5 psi instead of 50 psi).

Flow rate 
$$Q = Av$$
 where  $A = \frac{\pi d^2}{4}$  so that  $Q' = 1000 \ Q$ .

These relationships, together with typical ink jet values, dictated the design of the 100-fold scaled-up system as described below.

## • Unscaled parameters

Three effects are discussed here, i.e., the obvious gravity effects, the effects of the ambient atmosphere and heat conductivity effects.

Gravity Being a body force, gravity does not alter nozzle flow. All fluid elements feel the same acceleration regardless of their position or velocity. In fact, the gravity term in the equations of motion, Eq. (1), can be lumped into the hydrostatic pressure term so that its effect is merely to change the effective pressure, i.e.,

$$\mathbf{g} = -\nabla\phi \rightarrow \mathbf{g} - \frac{1}{\rho}\nabla p \equiv -\frac{1}{\rho}\nabla(p + \rho\phi) = -\frac{1}{\rho}\nabla p_{\text{eff}}.$$

Gravity effects on a free-falling vertical jet are more complicated. As the jet accelerates it also necks down so as to maintain a constant flow rate (the continuity equation). There are no effects at all on jet directionality. However, the jet's varying diameter has an impact on jet instability observations. This is because the exponential growth-rate of the jet's instability is a function of the jet's diameter. Consequently, the instability characteristics of a vertical jet undergoing break-up change with distance from the nozzle. This problem can be ignored if the break-up length of the jet is sufficiently short. Otherwise these effects have to be taken into account at the data reduction stage.

Ambient atmosphere The influence of the ambient fluid (air) is controlled by the ambient Weber number  $W_a = \rho_a v^2 d/\sigma$  where  $\rho_a$  is the ambient fluid density. Consequently  $W_a = (\rho_a/\rho) \ (\rho v^2 d/\sigma) = (\rho_a/\rho) \ W$  where W is the jet's Weber number. Since the ambient fluid is the same for both the prototype and scaled-up system and since W is fixed in both systems and the densities of ink and scaled-up ink (see the following sections) are almost identical, the ambient  $W_a$  is practically conserved and ambient atmospheric effects are therefore properly scaled.

Heat conduction As mentioned in the previous section, heat conduction effects are negligible in typical ink-jet printing devices.

The water-based inks used in ink jet printing display, typically, low thermal diffusivity resulting in temperature that is constant in time as well as in space.

# • Typical values

Typical values for ink jet printers are (at room temperature)  $d = 3 \times 10^{-3}$  cm;  $v = 2 \times 10^{3}$  cm/s;  $\rho = 1$  g/cm<sup>3</sup>;  $\mu = 1.8 \times 10^{-2}$  poise; and  $\sigma = 43$  dyne/cm (a typical static value). Therefore,  $R = \rho v d/\mu = 333$ ,  $W = \rho v^2 d/\sigma = 279$ , and  $F = v^2/g d = 1.3 \times 10^6$ .

These values may vary from one case to another so that the range of Reynolds numbers covered may be from 100 to 1000; Weber numbers from 100 to 400 and Froude numbers from  $4 \times 10^5$  to  $2 \times 10^6$ . For this reason the reported measurements cover a wide range of the most relevant indicator which, for directionality measurements, is the Reynolds number. Instead of R and W it is convenient for practical reasons to use other combinations of these:

$$L = \frac{W}{R} = \left(\frac{v}{\sigma/\rho}\right) v = 0.84$$

(L is independent of geometry), and

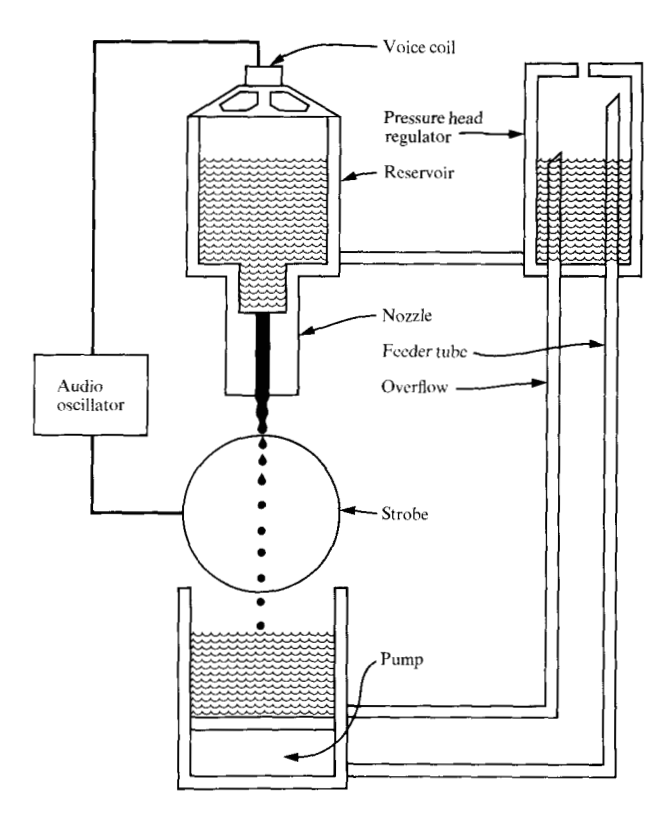


Figure 1 Schematic diagram of the scaled-up liquid jet system.

$$N = \frac{W}{R^2} = \left(\frac{v^2}{\sigma/\rho}\right) \frac{1}{d} = 2.5 \times 10^{-3}$$

(N is independent of velocity).

In practice, the kinematic viscosity  $\nu$  (a sensitive function of temperature) is varied to yield the desired N and then the velocity v is adjusted to yield the specified L. Thus R and W (or L and N) can be easily prescribed through simple temperature and pressure controls.

#### • The scaled-up "ink"

An acceptable room-temperature scaled-up ink was found to be ethylene glycol (HOCH<sub>2</sub>CH<sub>2</sub>OH) having R. T. properties of  $\rho = 1.11 \text{ g/cm}^3$ ;  $\mu = 19.9 \text{ centipoise}$  and  $\sigma = 47.7 \text{ dyne/cm}$ . These yield (at R. T.)

$$\frac{\nu}{\sigma/\rho} = \frac{\mu}{\sigma} \approx 4.2 \times 10^{-3} \text{ s/cm}$$

and

$$\frac{v^2}{\sigma/\rho} = 7.4 \times 10^{-4} \text{ cm}.$$

Consequently R. T. operation is possible at a scaled velocity of v = 200 cm/s.

**5**9

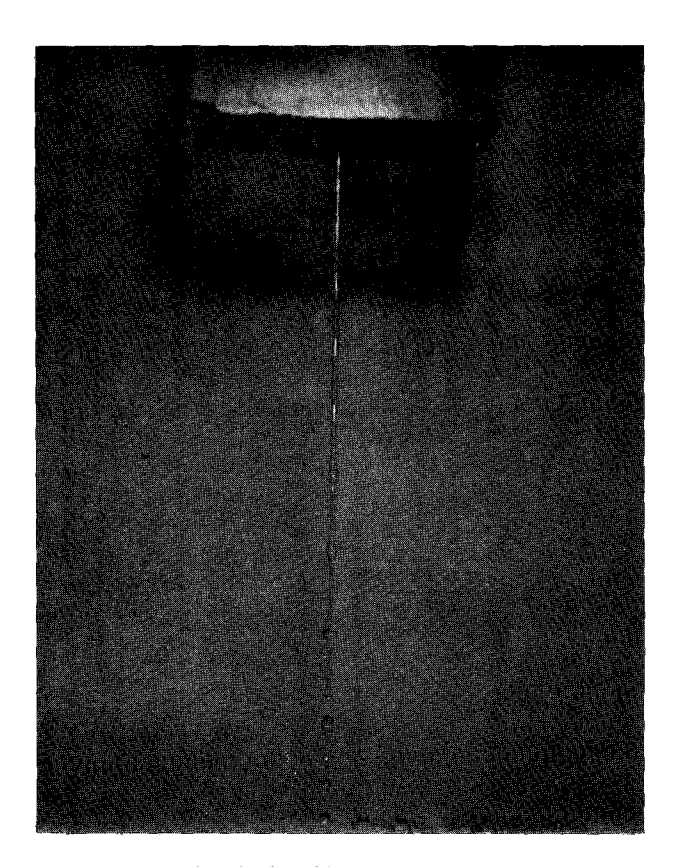


Figure 2 Scaled-up jet instability.

# **Experimental apparatus**

Once the scaling-up factor has been chosen (100 fold) and a proper scaled-up ink selected (ethylene glycol), the experimental apparatus can be built. In the design of the system care was taken to make flow observations, both inside and outside the scaled-up nozzle, as simple as possible. This required that the optical (refractive) index of the nozzle material be matched to ethylene glycol (n=1.43). Because the relevant flow parameters were controlled by temperature and pressure-head, a good stable flow-control is essential. Also, the scaled-up flow rate is 1000 times that of the prototype, while the scaled-up frequency is 0.001 of the original frequency (typically  $100 \, \text{kHz}$ ). The experimental set-up, described below, met all these requirements and in addition was simple to construct and operate.

## • Experimental set-up

The scaled-up system is shown in Fig. 1. It consists of the following:

1. Temperature controlled [ $(-20^{\circ}\text{C to } + 70^{\circ}\text{C}) \pm 0.1^{\circ}\text{C}$ ] bath and circulator (Forma Scientific Inc. Model 2095-SCR).

- 2. Nozzle support, mounted on a servo table.
- A constant head reservoir utilizing an adjustable overflow tube for pressure-head control.
- 4. A settling tank on top of which the acoustic speaker used for jet excitation is mounted. An optional mesh screen assembly can be added to the bottom of this tank to remove circulation and unsteady flow components.
- 5. A 100-fold scaled-up nozzle, molded from Sylgard 182 potting and encapsulating compound (Dow Corning). This material is easily molded using proper masters. Also, its optical index of refraction, n = 1.43, is the same as that of ethylene glycol, allowing observation of nozzle flow without optical distortion.

The experimental set-up described above proved to be extremely stable and free of external (interfering) vibrations. This fact, together with the larger dimensions involved, made accurate and systematic measurements possible.

#### • Excitation and visualization

As mentioned earlier the scaled-up frequency is approximately 100 Hz. This frequency is near the lower end of audio speakers. A 2.5-watt 6-in. speaker driven by a Crown DC-300 amplifier provided adequate excitation. Synchronous droplet observation was achieved with a strobing technique, using a stroboscope (GR model 1538 A) driven by a multiflash generator (GR model 1541). A function generator (Hewlett-Packard model 3311A) was used to drive both the excitation and the visualization circuits.

The stability of this system is illustrated in Figs. 2-4. In Fig. 2 the progress of the scaled-up jet instability is shown. Figure 3 displays the process of jet breakup and satellite formation, by observation of four consecutive wavelengths. A closeup of a jet break-up process is depicted in Fig. 4 where the jet was observed just before breakup, at the instant of breakup and just after breakup (a, b, and c, respectively).

## Measurement and procedures

The series of measurements reported below are devoted to directionality (jet initial aiming), directional stability (aim change with flow parameters), and flow efficiency (entrance effects on discharge coefficient). With these in mind, the only gravity effect which need be considered is that on jet directionality.

## • Gravity corrections

Measurements affected by gravity were corrected based on the following expression:

$$\frac{gx}{v_0^2} = \sin\phi \left( \sqrt{\cos^2\phi + \frac{2gH}{v_0^2}} - \cos\phi \right), \tag{8}$$

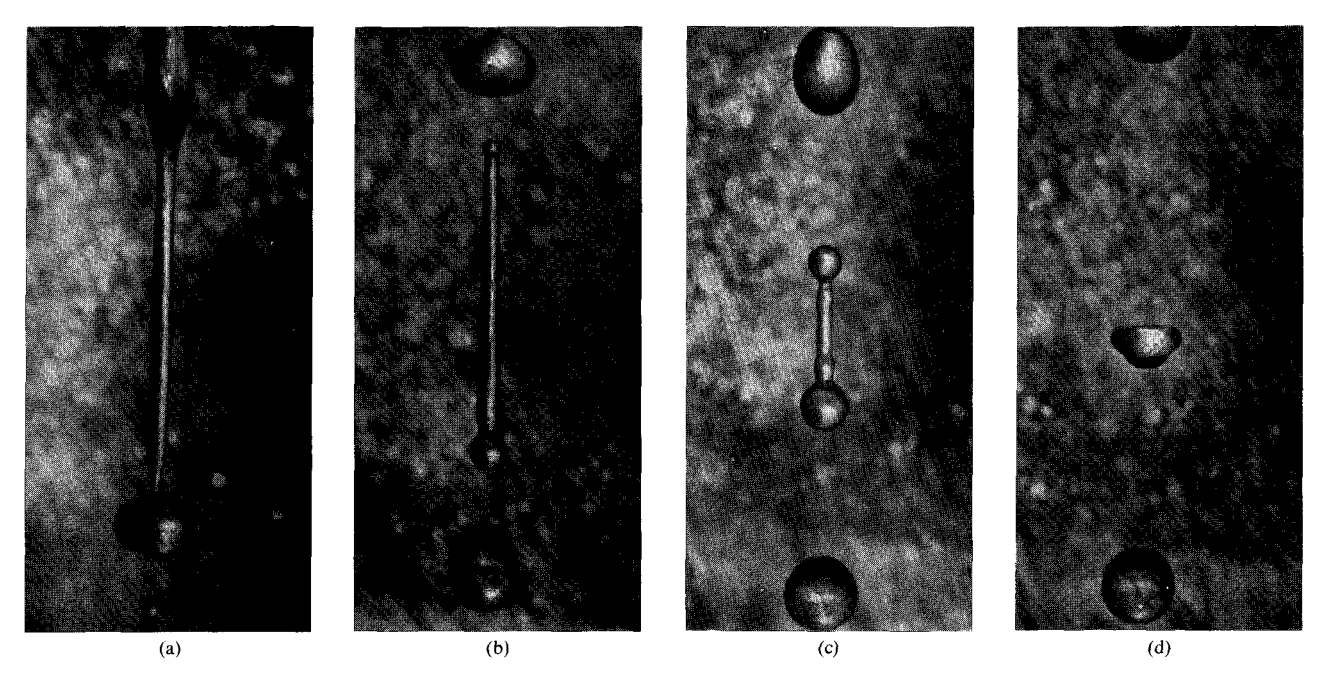


Figure 3 Jet breakup and satellite formation showing four consecutive wavelengths (see text).

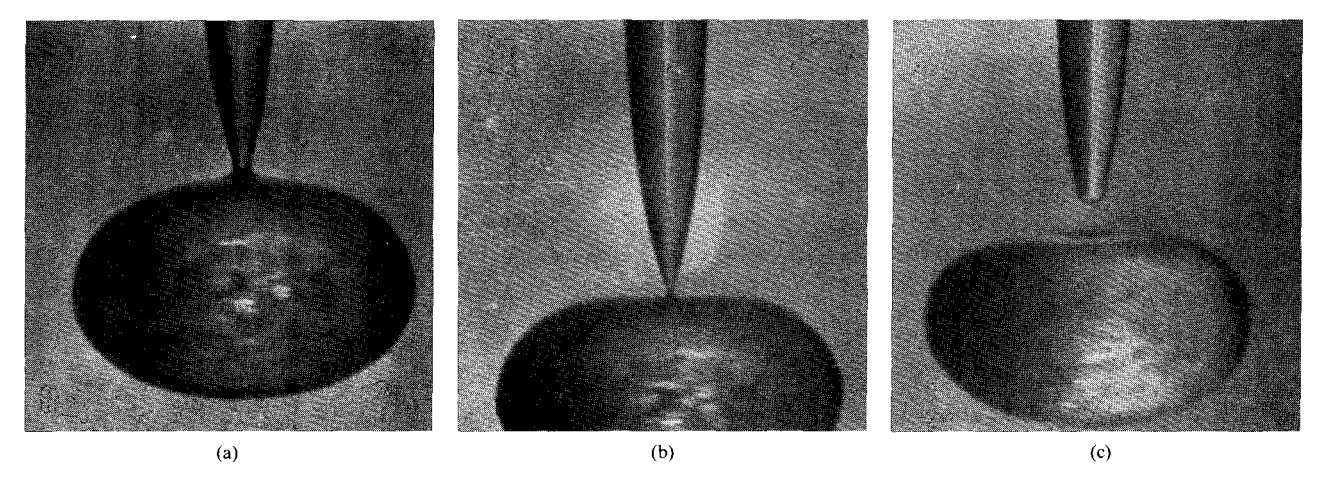


Figure 4 The jet breakup process (before, at and after breakup).

in which g is the jet acceleration due to gravity, x is the observed jet linear deflection at the reference plane,  $v_0$  is the jet initial velocity, H is the nozzle height above the reference plane, and  $\phi$  is the jet deflection angle. Equation (8) was used to translate the linear deviations, measured at the reference plane, into the corresponding deflection angles. The negligible effect of air resistance in this set-up was not considered.

# • Measurement accuracy

Since, in practice, deflection angles of only a few milliradians are expected, it is important to evaluate the accuracy of results based on Eq. (8). A generous estimate of the linear deviation would be  $\delta x = 2.5$  mm (0.1 in.), i.e., a reading error of better than 2.5 mm. Translated into angular deflection accuracy, it corresponds to less than 1 milliradian. This result is based on a nozzle to reference plane distance H = 114 cm (1.14 cm for the prototype) and a jet velocity of  $v_0 = 166$  cm/s (1660 cm/s or 660 in./s for the prototype).

## • Experimental procedure

All directionality measurements were performed at a reference plane placed 45 in. (114 cm) below the nozzle

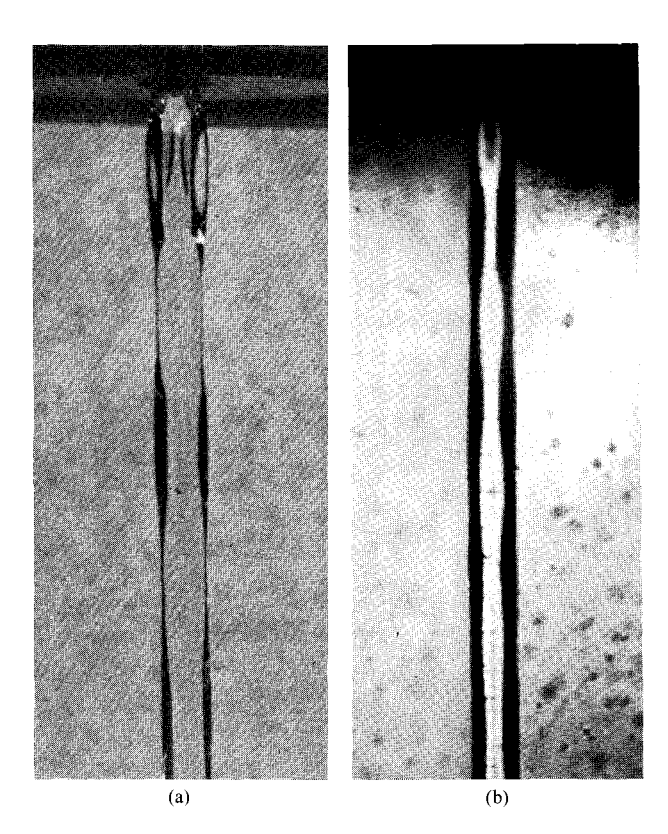
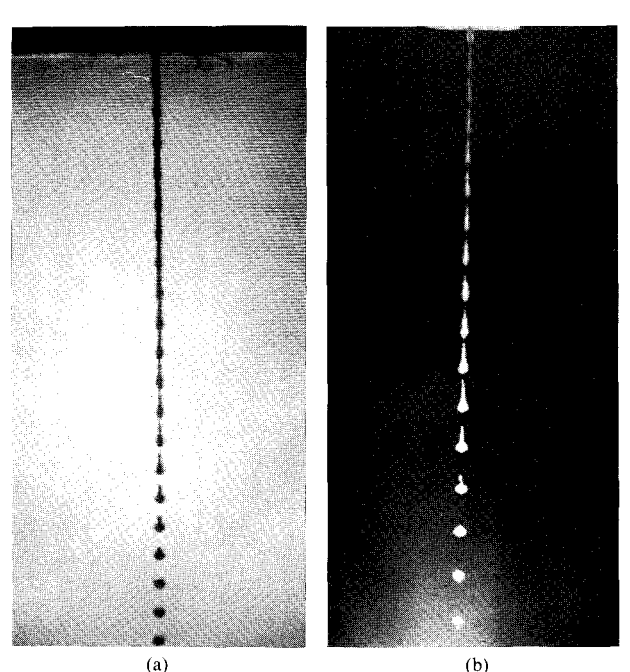


Figure 5 Unexcited jet from square nozzles: (a) scaled up and (b) prototype.

Figure 6 Comparison of a prototype (a) and a scaled-up (b) jet. Gravity effects are apparent in (b).



exit. A scale, graded in millimeters and placed at the reference plane, was used for all linear deviation measurements. Care was taken to establish accurately the zero deviation point. Surface tension and viscosity checks were performed before and after measurements. Slight variations were found in viscosity due to H<sub>2</sub>O absorption. However, the changes were very slow compared to the time required to complete the series of measurements for each experiment. Mean fluid velocities were normally computed from flow-rate measurements using a 1000-ml container and a stopwatch. Results were confirmed by weighing the collected fluid. A small densitometer yielded accurate density results that were used to compute the flow rates. The system was extremely stable and all measurements repeatable.

#### **Experiments and results**

The experimental results reported here describe the effects of different nozzle configurations on the directionalities of jets emitted by these nozzles under varying operating conditions. Specifically, the experiments were designed to test the sensitivity of these nozzles to any deviation from their intrinsic symmetry. The effects of entrance conditions on flow efficiency and stability were also investigated. Flow efficiency can be described in various ways, i.e. mean velocity or flow rate. However, two dimensionless parameters are normally used. These are the discharge coefficient  $C_{\rm D}$  and the nozzle coefficient  $\xi$ . The discharge coefficient is given by

$$C_{\rm D} = \frac{v_{\rm m}}{\sqrt{2p/\rho}} = \frac{v_{\rm m}}{\sqrt{2gh}} = \frac{v_{\rm real}}{v_{\rm ideal}},\tag{9}$$

where p is pressure,  $\rho$  is density, g is gravitational acceleration, h is pressure head and  $v_{\rm m}$  is measured mean fluid velocity.

The last equality follows from the fact that the denominator equals the fluid velocity under ideal conditions, i.e. under no-loss conditions. In this case  $P=\frac{1}{2}\rho v_{\rm ideal}^2$  and hence  $v_{\rm ideal}=\sqrt{2\rho/\rho}$ . The nozzle coefficient is defined as

$$\xi = 1/C_{\rm p}^2 = 2p/\rho v_{\rm m}^2. \tag{10}$$

This parameter is more convenient to use for analysis in some cases.

# • Verification of model

The theoretical model described above asserts that, with the exception of gravity, scaling up may be achieved through simple control of Reynolds and Weber numbers. All other parameters, which are not scaled, have a negligible effect and can be ignored. To test the applicability of such a model, a series of measurements on both the prototype and the scaled up model is required. In those cases where it was possible, such measurements were performed and resulted in satisfactory agreement. Some



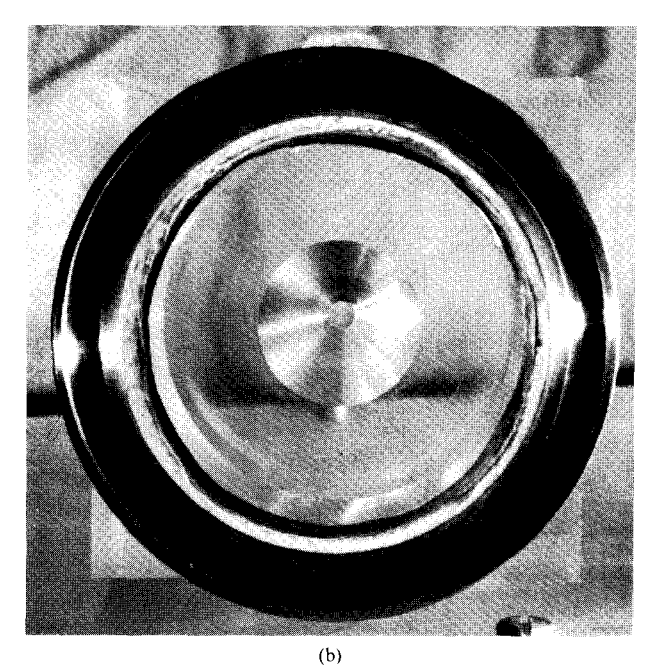


Figure 7 Photographs of a scaled-up conical nozzle. (a) Side view; (b) end view.

results first observed on the scaled-up system were later confirmed in experiments performed on prototype nozzles. Interesting observations on square nozzles are shown in Figs. 5(a) and 5(b) (scaled up and prototype, respectively). The emitted jet starts as a square and oscillates about its cylindrical equilibrium shape. The period of oscillation scales properly ( $6 \mu s$  scales to 6 ms). Figure 6 displays a comparison of the breakup process in a prototype (a) and the 100-fold scaled up version (b). Again the similarity is obvious. The effects of gravity are beginning to become noticeable as the distance from the nozzle increases, Fig. 6(b).

## · Conical nozzles

This nozzle configuration, Fig. 7, consists of a conical section nominally 50° half angle (but ranging from 20° to 80°), terminated by a circular cylindrical section. These nozzles, commercially available, are manufactured from watch jewels and were an early choice in the development of ink jet printing. Fabrication of "jewel" nozzles consists, typically, of four steps as follows:

- 1. cone drilling, using conventional high speed drills;
- 2. orifice drilling, using ultrasonic drilling of the cylindrical section;
- 3. nozzle polishing, using thin wires and slurry; and
- 4. lapping and polishing of the nozzle "face" to the desired length and finish. (This step is normally performed by the user.)

The above mentioned procedure does not yield reproducible results and hence an additional step of optical inspection and selection is normally introduced. The final test must be a functional one because optical inspection is incapable of identifying minute imperfections and/or asymmetries, giving rise to poor directional performance. Indeed, it has been found experimentally that a nozzle which looks good does not necessarily perform well. Sectioning of jewel nozzles failed to reveal a correlation between optical selection (except for gross imperfections) and nozzle performance.

Nozzle shapes encountered in practice include varying cone angles, parabolic rather than conical walls, and orifice/cone misregistration and misorientation. Scaledup versions of these irregular types were fabricated and tested first for flow efficiency (characterized by the discharge coefficient). Nozzles were tested with the conical sections serving both as entrances and as exits. In addition, for comparison purposes, flow-efficiency curves were plotted for two (straight) cylindrical nozzles; one had a sharp entrance condition whereas the other had an appreciable entrance rounding. The results are summarized in Figs. 8 and 9. The Reynolds number is plotted vs head pressure in Fig. 8 and the discharge coefficient vs head pressure is given in Fig. 9. It should be noted that the nozzles divide themselves into two groups; those with high discharge efficiency ( $C_{\rm D} > 0.7$ ) and those displaying poor flow efficiency ( $C_{\rm p} < 0.7$ ). It is interesting to note that, invariably, poor flow efficiency is linked to

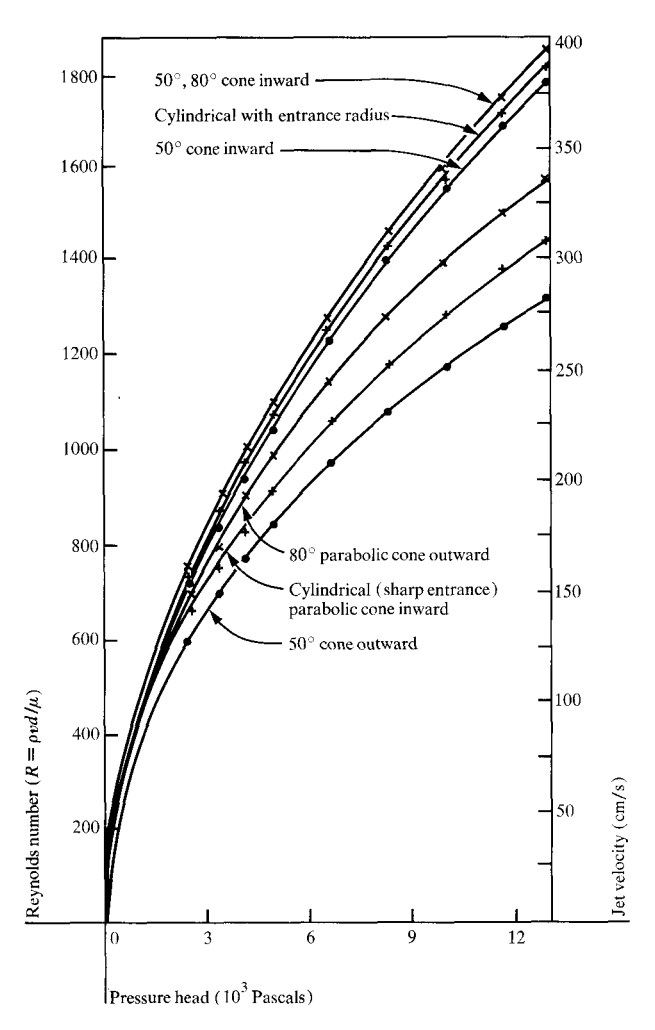


Figure 8 Reynolds number vs head pressure for conical nozzles. For comparison purposes data for two cylindrical nozzles with different entrances are shown.

sharp entrance conditions, whereas high flow-efficiency nozzles must have a flow-preparation entrance region (a cone or entrance rounding). Observations made during the course of measurement revealed that all sharpentranced nozzles exhibited directional instabilities, evidenced in two forms. First, at a constant pressure head the jet stream kept fluttering minutely and second, as the head was slowly and continuously changed, jet directionality suffered abrupt and relatively large (10-15 milliradians) changes.

# • Cylindrical nozzles

The cylindrical nozzle configuration, Fig. 10, consists of a circular cylindrical shape with a prescribed degree of entrance rounding. Raw material (glass) for these nozzles is available commercially but not to the precision required for good reproducible performance. The fabrication process consists normally of the following steps:

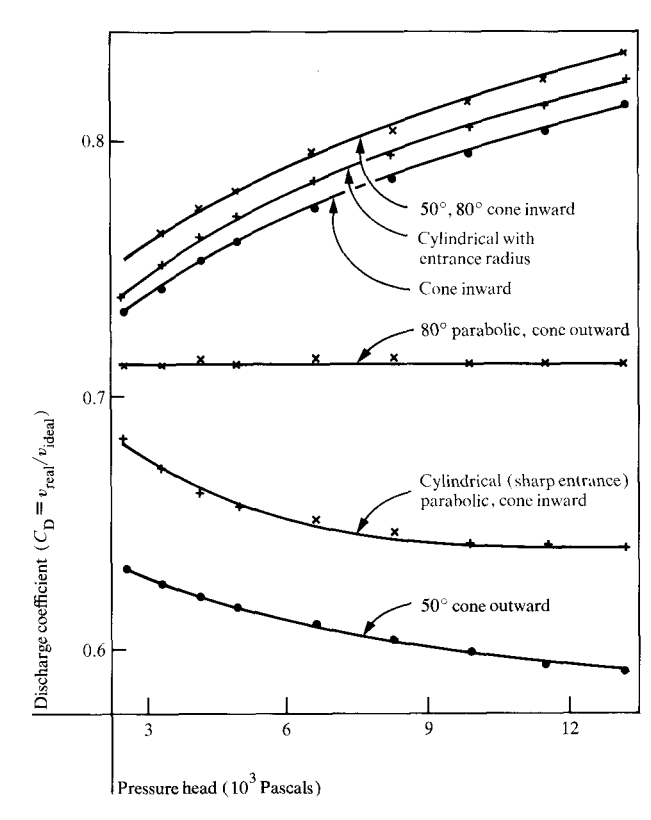


Figure 9 Discharge coefficient,  $C_{\rm D}$ , vs head pressure for conical nozzles. Results for two cylindrical nozzles are included.

- 1. glass-tube pulling, using a specially designed furnace (reduces sizes to required specifications);
- slicing and lapping, using conventional equipment (prepares samples for polishing);
- nozzle polishing, using soft pads for final surface finish and long hair pads for entrance rounding; and
- 4. nozzle mounting, using epoxy or glassing directly to the adaptor plate.

This procedure yields good, reproducible results. Care must be exercised in, first, the choice of glass (to minimize corrosion caused by the ink); second, a lower limit on nozzle length due to the fragility of thin glass wafers; and last, control of entrance rounding. Functionally these potential problem areas were found to be readily controlled through precise, careful material selection and process control.

To test the effects of entrance conditions on frozzle performance, seven scaled-up cylindrical nozzles were fabricated with different degrees of entrance rounding radii. All nozzles had an I.D. of 5.1 mm (0.2 in.) and a length of 5.1 mm (aspect ratio of 1) but entrance radii of "sharp," 0.063 mm, 0.127 mm, 0.190 mm, 0.253 mm, 0.38 mm, 0.51 mm and 0.77 mm, respectively. Flow efficiency measurements yielded the results depicted in

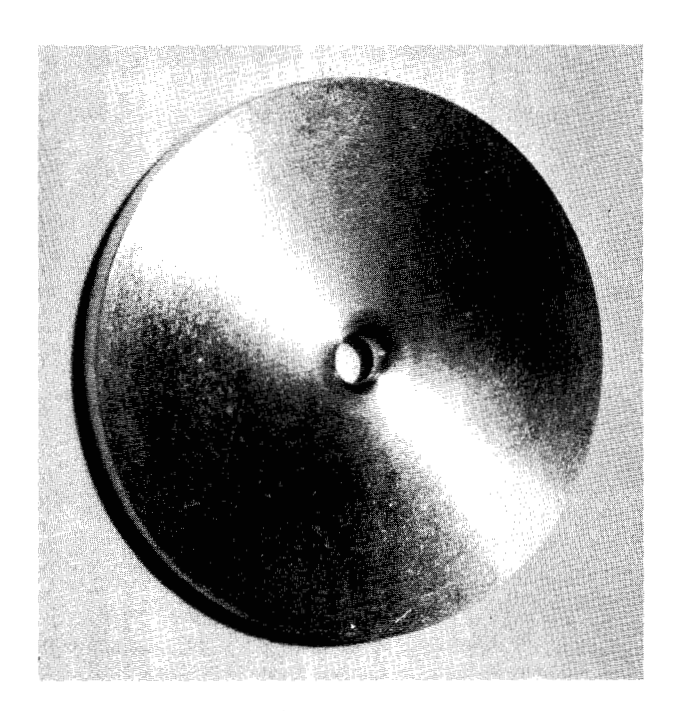


Figure 10 Photograph of a circular cylindrical nozzle.

Figs. 11, 12 and 13. It is evident from these figures that the different nozzles can be classified in two distinct groups. Those with entrance radii of 3.75 percent of the I.D. or larger follow the normal pattern, i.e., flow efficiency increases with pressure head. Its rate of change, however (slope of  $C_{\rm p}$  in Fig. 11), decreases with head. On the other hand, nozzles whose entrance radii are 2.5 percent of I.D. or less exhibit an abnormal behavior. Their flow efficiency is either insensitive or actually decreases with pressure head at the lower heads, and is constant at the higher values. In addition, these sharpentranced nozzles display directional instabilities (similar to those mentioned earlier) at the lower heads (below 61 cm of ethylene glycol). The flow-efficiency pattern of the different nozzles can be further clarified when Fig. 12 is considered. Here the nozzle coefficient  $\xi = 1/C_D^2$  is plotted against the reciprocal Reynolds number. Clearly, data points are best fitted to straight lines. This means that the nozzle coefficient can be expressed mathematically as  $\xi = A + (B/R)$  (R = Reynolds number), where Aand B are constants determined by the nozzle's aspect ratio and entrance radius.

The effects of entrance rounding for the nozzles tested (all having a geometrical aspect ratio of 1) are shown in Fig. 13 in the limit of high Reynolds numbers. It is seen that the empirical limit of  $\xi = 1.3$  is rapidly approached. Therefore, in this limit (large R), entrance radii of 10-15 percent of nozzle I.D. are sufficient to minimize entrance losses, and further rounding will have little effect on flow

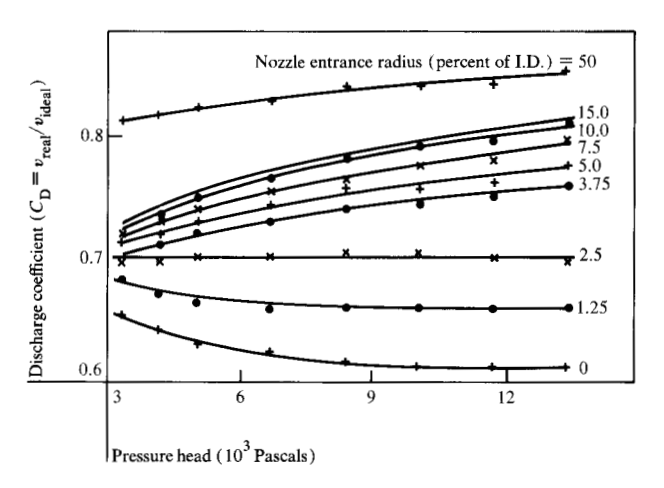


Figure 11 Discharge coefficient,  $C_{\rm D}$ , vs head pressure for cylindrical nozzles.

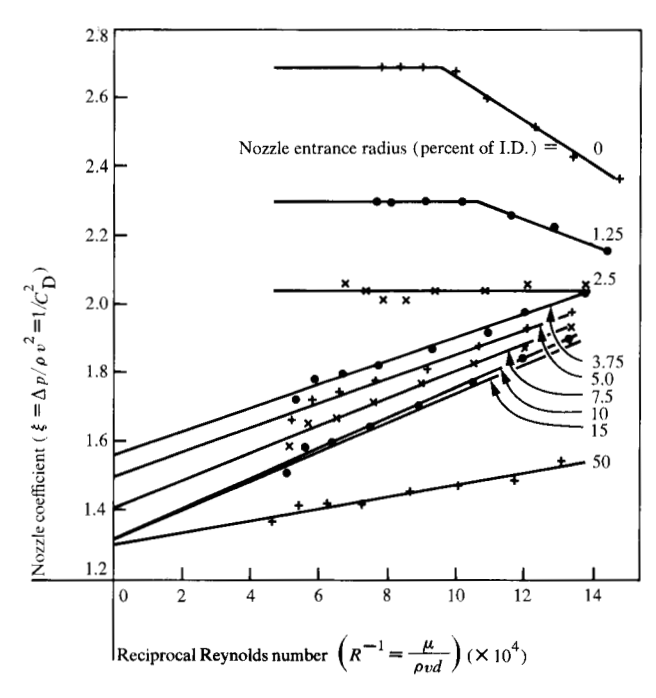


Figure 12 Nozzle coefficient,  $\xi$ , vs reciprocal Reynolds numer for cylindrical nozzles.

efficiency. (These points will be discussed later in detail.) Entrance rounding, however, has an increasing effect on flow efficiency as the Reynolds number decreases. The abnormal behavior of the sharp nozzles can be explained in terms of competition between flow separation, which occurs at the higher Reynold numbers, and flow reattachment, which dominates the low region of Reynolds numbers. This is discussed later in this report.

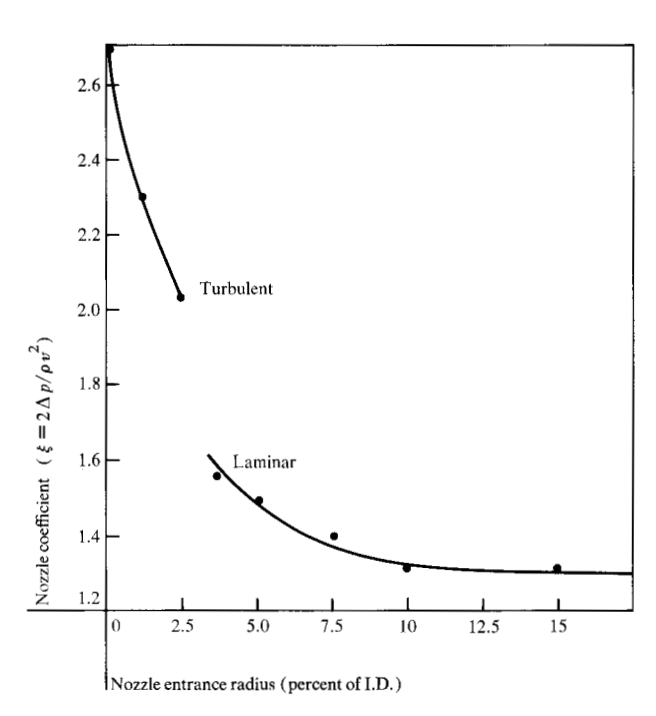


Figure 13 Nozzle coefficient,  $\xi$ , vs entrance radius for cylindrical nozzles (at the limit of large Reynolds numbers).

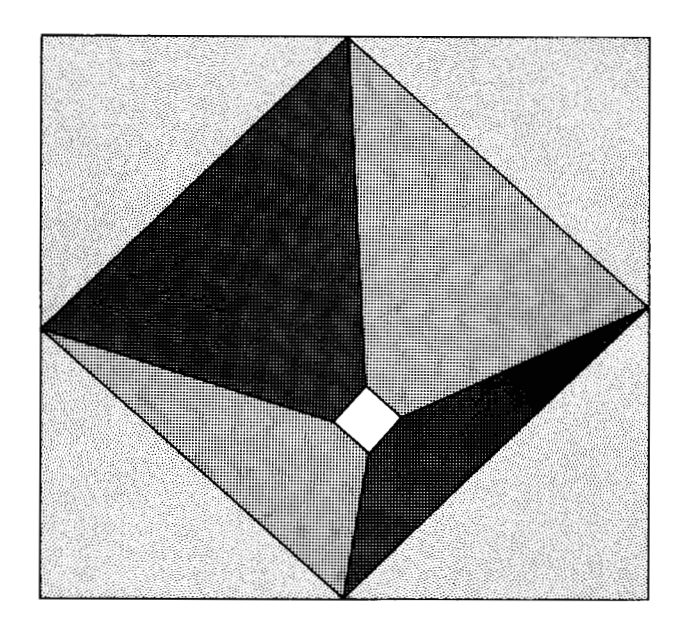


Figure 14 Drawing of a square nozzle, showing the pyramidal entrance region and square orifice.

## • Square nozzles

This nozzle configuration, Fig. 14, is the square equivalent of the conical nozzle and consists of a truncated pyramid. Like the conical nozzle it displays good flow

**Table 1.** Values of the dimensions of the scale-up and prototype hybrid nozzles.

Parameter	Scale-up (mm)	Prototype (mm)
Membrane size	9.6 × 9.6	$0.096 \times 0.096$
Orifice diameters	2.0	0.02
	2.5	0.025
	3.0	0.03
	3.6	0.036
	4.6	0.046
Nozzle length	0.76	0.0076
Reference plane (below orifice)	1140.	11.40
Jet velocity	168 cm/s	1680 cm/s

efficiency. The lack of a final straight exit section in such a nozzle makes this configuration directionally sensitive to any asymmetries (imperfections) in its structure. It is interesting to note that isolated, localized flaws have been found to affect jet directionality appreciably less than even small departures from structural symmetry. This somewhat unexpected behavior (also observed in the other, less sensitive, configurations) suggests that jet directionality may be defined by the overall nozzle symmetry rather than the appearance of suspicious-looking localized flaws.

The performance of a square orifice is interesting, especially near its exit where a square jet, Fig. 15, is emitted. This jet oscillates about its equilibrium cylindrical shape due to surface tension forces. Viscosity dampens these oscillations so that normally there is no trace of this effect at the jet's breakup time. It is, however, still an open question whether this phenomenon has any influence on the process of satellite formation, which is determined much earlier than breakoff time. The frequency of these oscillations was found to be approximately 160 Hz for a jet of diameter 0.25 cm and mean velocity of 100 cm/s. Consequently, the oscillation's wavelength was approximately 0.6 cm or about 2.4 diameters. This value is below the critical value of  $\pi$  diameters for the onset of instability. Therefore, the jet is stable against these noncylindrical perturbations and indeed recent investigations have, so far, failed to reveal any negative effects on jet performance in general and the breakup process in particular.

# Hybrid nozzles

This nozzle configuration, Fig. 16, is a combination of the square (pyramid) type entrance and a circular cylindrical orifice. The orifice is located at the geometrical center of a thin plate (the membrane) which caps the truncated

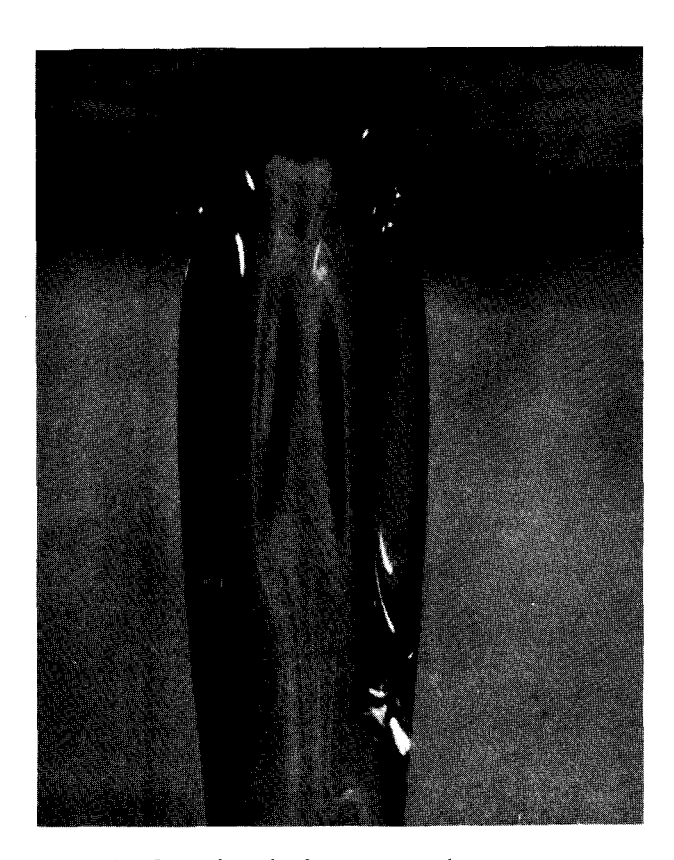


Figure 15 Jet at the exit of a square nozzle.

pyramid entrance. When the (pyramid) side walls are sufficiently removed from the orifice, their effect can be ignored. The nozzle then performs as a straight cylindrical nozzle with a very small aspect ratio. The relationship between orifice misregistration (with respect to the pyramid's geometric center) and jet directionality is of obvious importance since it determines the usefulness of such nozzles. The experimental set-up consists of a vertically mounted hybrid nozzle positioned at a height of 114 cm (45 in.) above the reference plane at which jet deflection from the vertical was observed. The micrometer-driven orifice plate was pressure mounted onto the nozzle body using silicone coating to ensure smooth motion of the plate with respect to the pyramidal entrance region. Data were collected, analyzed and corrected for gravity effects following the steps described earlier.

The scaled-up experimental conditions and the corresponding prototype values are given in Table 1. The results are plotted in Fig. 17. The expected dependence of the deflection sensitivity on the ratio of orifice diameter to membrane size is readily observed. Also the increased sensitivity (slope) with misregistration is clearly demonstrated. In Fig. 17, orifice misregistration is defined as the ratio of the distance between the orifice center and the membrane center to half the square of the membrane length.

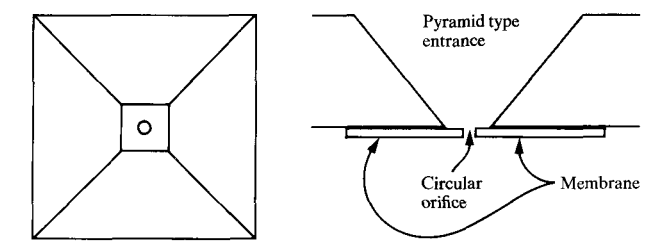


Figure 16 Schematic diagram of the hybrid nozzle.

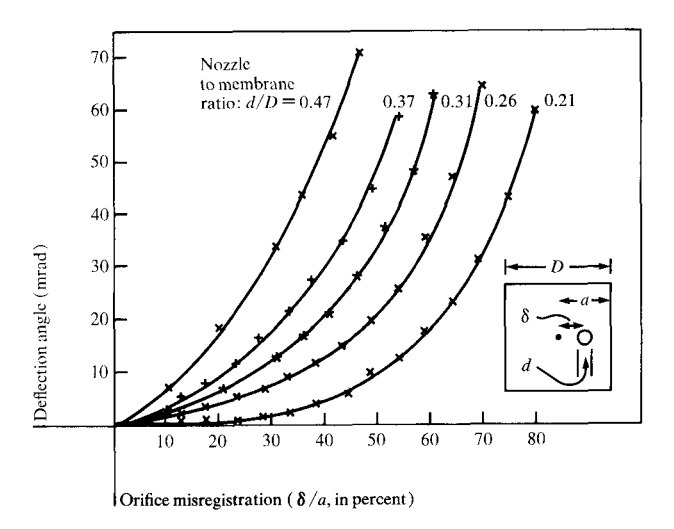


Figure 17 Directionality effects in hybrid nozzles, showing deflection angles vs orifice misregistration.

Although these measurements were taken at a jet velocity of 168 cm/s (66 in./s), they do not vary significantly with velocity. Under worst-case conditions (orifice-"touching" membrane edge and the velocity cut in half), deviation decreased by less than 10 percent. Flow rate was similarly insensitive to orifice misregistration, except very close to the membrane edge.

#### Discussion

Four different nozzle configurations have been considered. Their flow-efficiency characteristics and their effects on jet directionality have been investigated. The results for cylindrical nozzles are particularly interesting because of available analysis on entrance effects in cylindrical pipes. Hamilton [5] investigated the effects of entrance rounding on intake losses in pipe flow. His result is that "full suppression of intake loss occurs with radius of rounding equal to 14 percent of the pipe diameter." Hamilton's experiments were performed on large pipes with large Reynolds numbers. The results depicted in Fig. 13 confirm Hamilton's findings in the limit of

large Reynolds numbers. However, Fig. 12 shows that as the Reynolds number decreases (i.e. its reciprocal increases), Hamilton's result becomes increasingly less accurate. This is evident from the divergence of the 50 percent rounding (ideal) nozzle curve with respect to the others as the reciprocal of the Reynolds number increases. The excellent straight-line fit to the data in Figure 12 leads (as mentioned earlier) to the relation:  $\xi = 2\Delta P/\rho v^2 = A + (B/R)$ . This expression has the functional form suggested by Holmes [6] for the treatment of entrance losses, and used by Sylvester and Rosen [7] and by Kaye and Rosen [8] to discuss sharp entrances. In the case of nozzle flow, the pressure drop across the nozzle (from nozzle entrance to jet stream) can be written as

$$\Delta p \cong \varepsilon_{\text{kinetic}} + \varepsilon_{\text{surface}} + \varepsilon_{\text{viscosity}} + \varepsilon_{\text{loss}}$$

where the  $\epsilon$  are energy losses (per unit volume) due to various causes, and are given by

$$\varepsilon_{kin} = K \cdot \frac{1}{2}\rho v^{2},$$

$$\varepsilon_{surf} = \frac{2\sigma}{d} = \frac{4}{W} \left(\frac{1}{2}\rho v^{2}\right),$$

$$W = \rho v^2 d/\sigma$$
 (Weber);

$$\varepsilon_{\text{visc}} = 32\mu l \frac{v}{d^2} = \left(\frac{64}{R} \frac{l}{d}\right) \left(\frac{1}{2}\rho v^2\right),\,$$

 $R = \rho v d / \mu$  (Reynolds); and

$$\varepsilon_{\text{loss}} = K' \frac{\mu v}{2d} = \frac{K'}{R} \left( \frac{1}{2} \rho v^2 \right).$$

Therefore

$$\xi = \frac{\Delta p}{\frac{1}{2}\rho v^2} = K + \frac{K'}{R} + \frac{64}{R} \frac{l}{d} + \frac{4}{W}.$$

The first two terms [K + (K'/R)] are normally considered to be the entrance loss. Here K and K' are functions of entrance rounding as well as nozzle aspect ratio (l/d). Specificially, K and K' are correction coefficients for velocity profiles that are not fully developed. This means kinetic, as well as viscous, loss corrections. For fully developed flow, kinetic energy considerations alone predict K = 2.0 (because  $\overline{v^2} = 2\overline{v}^2$  for parabolic flow). Experimentally, the value K = 2.3 has been found to best fit the data. Flow through a sharp entranced nozzle should therefore yield K = 1.3 (compared to the predicted K=1). Figures 12 and 13 verify that in the limit of high Reynolds numbers this limit is rapidly approached with entrance radii larger than 10-15 percent of nozzle I.D. However, as the Reynolds number decreases, entrance rounding can still improve nozzle flow characteristics. Another interesting phenomenon exhibited in Fig. 12 is the pattern displayed by the three sharp-entranced nozzles (rounding less than 2.5 percent of I.D.). These three nozzles were extremely directionality sensitive, especially at the *lower* Reynolds numbers (R < 1000). At large Reynolds numbers (R > 1000) they were insensitive to pressure variations and therefore can be explained in terms of separated flow. As the Reynolds number decreases, competition between flow separation (supported by the inertial forces) and flow reattachment (to the nozzle wall) increases. At Reynolds numbers of 1000 and smaller, flow reattachment takes place as evidenced by directionality changes observed in the experiments. As R is further decreased, the size of the contracted flow (the so-called "vena-contracta") decreases so that flow efficiency increases towards its optimum value of non-separated laminar flow.

## **Acknowledgments**

The author thanks J. B. Little and A. H. Kendall for suggesting and encouraging this project, R. Schaffer who collaborated on some of the experiments, A. R. Hoffman who helped in the initial stages, and, finally, W. W. Hildenbrand whose design ingenuity made experimentation a simple and pleasant experience.

#### References

- S. A. Curry and H. Portig, "Scale Model of an Ink Jet," IBM J. Res. Develop. 21, 10 (1977, this issue).
- For example, H. Schlichting, Boundary Layer Theory, McGraw-Hill Book Company, Inc., New York, 1960.
- 3. C. A. Bruce, "Dependence of Ink Jet Dynamics on Fluid Characteristics," *IBM J. Res. Develop.* 20, 259 (1976).
- E. B. Christiansen and S. J. Kelsey, "Nonisothermal Laminar Contracted Flow," *AIChE J.* 18, 713 (1972).
   J. B. Hamilton, "The Suppression of Intake Losses by Vari-
- J. B. Hamilton, "The Suppression of Intake Losses by Various Degrees of Rounding," Univ. Wash. Expt. Sta. Bull. 51 (1929).
- D. B. Holmes, Ph.D Dissertation, Delft University, Netherlands (1967).
- N. D. Sylvester and S. L. Rosen, "Laminar Flow in the Entrance Region of a Cylindrical Tube," AIChE J. 16, 964 (1970).
- S. E. Kaye and S. L. Rosen, "The Dependence of Laminar Entrance Loss Coefficients on Contraction Ratio for Newtonian Fluids," AIChE J. 17, 1269 (1971).

Received July 9, 1976

Dr. M. Levanoni is a member of the manufacturing research group of the IBM System Products Division and is located at the IBM Thomas J. Watson Research Center, Yorktown Heights, NY 10598.